Toward 4-D Trajectory Management in Air Traffic Control: A Study Based on Monte Carlo Simulation and Reachability Analysis

Kostas Margellos, *Student Member, IEEE*, and John Lygeros, *Fellow, IEEE*

***Abstract*— One of the fundamental elements for the next generation in air traffic management systems, as envisioned by the Single European Sky Air Traffic Management Research Project and the Next Generation Air Transportation System Project, is 4-D trajectory management. In the contract-based air transportation system project, a novel concept of operations based on target windows (TWs) is developed. TWs are 4-D constraints imposed at different parts of the flight to increase predictability, efficiency, and safety. In this paper, we use Monte Carlo simulations and reachability analysis to evaluate some of these features of the TW concept. We start by using Monte Carlo methods to estimate the TW hitting probability and the probability of conflict. We then outline methods and computational tools based on reachability theory and highlight how they can be adapted to characterize the maneuvering freedom afforded by TWs. We also demonstrate how the reachability calculations can be used to guide conflict resolution in the presence of TW constraints. Our results indicate that TWs provide a promising balance between predictability of air traffic and maneuverability.**

***Index Terms*— Air traffic control, conflict resolution, 4-D trajectory management, hybrid systems, Monte Carlo simulations, optimal control, reachability theory.**

I. Introduction

AIR TRAFFIC is expected to increase rapidly over the coming decades. This increase is expected to lead to further departure delays and en-route congestion [1], [2], which in turn might cause additional safety problems and lead to an increased number of conflicts compared to the current situation. A major issue when attempting to deal with this scenario is uncertainty about the future evolution of flights. The focus to reduce this uncertainty has shifted toward the so called 4-D trajectory management, which is widely regarded as the basis for the next generation in air traffic management systems envisioned by the Single European Sky Air Traffic Management Research (SESAR) [3] and the Next Generation Air Transportation System (NextGen) [2] projects.

The contract-based air transportation system (CATS) research project [4] proposed one possible implementation of the 4-D trajectory management concept, called the contract of objectives (CoO) [5]. The CoO provides objectives for each actor involved in a flight (air traffic controllers, airports, airlines, air navigation service providers), which represent their commitment to deliver a particular aircraft inside specific temporal and spatial constraints called target windows (TWs) [6]. The hope is that the TWs will help to increase predictability, punctuality, and safety during the flight. A detailed methodology for the computation of the TWs based on the constraints imposed by the various actors can be found in [6], and their importance from an airline perspective is investigated in [7].

The presence of TWs could potentially increase predictability, but also imposes additional constraints that air traffic controllers should respect when issuing conflict resolution maneuvers. TWs, therefore, represent a tradeoff between the predictability of flights (which tends to make the task of air traffic controllers simpler) and their maneuverability (which tends to make air traffic control more complex). As part of the validation effort of the CATS project, this tradeoff was investigated through human in the loop simulations (HIL) [8], [9]. Even though HIL simulations provide the most realistic way for the validation of the overall concept, they have several limitations, most notably their inability to quantitatively assess the probability of rare events, such as conflicts.

In this paper, we conduct a complementary computational study of this tradeoff between predictability and maneuverability achieved through TWs. We first use Monte Carlo simulations to assess the probability of flights meeting their TW constraints and the probability of conflict under TW operation in the realistic scale set-up used in the CATS HIL experiments. Monte Carlo simulations have been used extensively in air traffic control for optimization purposes [10], safety verification [11], [12], and to estimate the conflict probability due to wind uncertainty [13]–[15]. Even though highly sophisticated Monte Carlo methods [11] are not necessary in our case, since the events of interest have substantial probability, deployment of Monte Carlo methods still requires novel developments, such as a feedback controller to emulate the actions of air traffic controllers and pilots might take to meet TW constraints. Our results indicate that TW tracking is feasible even with the current fleet of aircraft, which are mostly equipped with the so-called 3-D flight management systems that do not automatically correct for timing deviations.

To assess the maneuvering freedom afforded by TWs, we propose a novel method based on the solution of a reachability problem with state constraints, a "reach-avoid" problem in the

Manuscript received June 19, 2011; revised August 28, 2012; accepted September 17, 2012. Manuscript received in final form September 21, 2012. Date of publication October 24, 2012; date of current version August 12, 2013. This work was supported in part by the European Commission under Project CATS FP6-TREN-036889 and the Network of Excellence HYCON2 under Project FP7-ICT-257462. Recommended by Associate Editor M. Prandini.

The authors are with the Automatic Control Laboratory, Department of Information Technology and Electrical Engineering, ETH Zürich, Zürich 8092, Switzerland (e-mail: margellos; lygeros@control.ee.ethz.ch).

Color versions of one or more of the figures in this paper are available online at http://ieeexplore.ieee.org.

Digital Object Identifier 10.1109/TCST.2012.2220773

sense of [16] and [17]. In the dynamics and the control literature, there are already numerous applications where reachability theory has been employed among others to problems in air traffic management [16], [18], [19], and flight control [20]–[24]. A common objective in most of these applications is to design controllers so as to reach a target set while satisfying state constraints. In the context of viability theory [25], these sets are known as capture basins [26]–[31]. In the presence of state constraints, reach-avoid problems for continuous systems were characterized in [17] as the viscosity solution to a quasi-variational inequality in the form of [32], based on the earlier work on unconstrained problems [33], [34]. The case of competing inputs was also considered in a reachability context in [35], using the appropriate notion of strategies proposed in [36]. To solve such problems numerically, algorithms based on level set methods have been developed [37], [38], and have been coded in computational tools [39], [40].

In the context of TW-based 4-D trajectory management, we build on previous work [41], [42], and perform a reach-avoid computation to construct conflict-free tubes. We then manually place an artificial TW inside each tube to initiate a resolution maneuver for each aircraft. Although not implemented in this paper, an optimization step could be included here to place the additional TWs in an optimal way and avoid situations where a subsequent conflict might occur. Automation in this process is not the main purpose of this paper though, which aims to illustrate how the maneuvering bounds determined by the reach-avoid tubes could be used as a decision support tool for air traffic controllers. The bounds can also serve as feedback to the TW generation process [6], to design less conservative TWs.

This paper is organized in five sections. Section II contains details regarding the modeling of the aircraft, the TWs, and the TW tracking controller. In Section III, some background information regarding the reachability analysis is provided, our simplified assumptions for the hybrid abstraction of the aircraft dynamics are stated, and the conflict resolution problem is formulated in the reachability framework. Section IV summarizes the simulation results obtained from the TW concept evaluation and the conflict resolution algorithm. Finally, in Section V, we provide some concluding remarks and directions for future work.

II. Mathematical Modeling

A. Simulation Environment

Both the continuous dynamics for the aircraft motion and the discrete events triggered by the FMS and the flight plan, are described in detail in [43]. Using this as a starting point, [44]–[46] develop a stochastic hybrid model for the flight dynamics. Following [43], we consider a six-state, flat earth, trimmed, point mass model for aircraft dynamics:

$$\dot{\mathbf{x}} = \begin{bmatrix} \dot{x} \\ \dot{y} \\ \dot{z} \\ \dot{V} \\ \dot{\psi} \\ \dot{m} \end{bmatrix} = \begin{bmatrix} V\cos\psi\cos\gamma + w_x \\ V\sin\psi\cos\gamma + w_y \\ V\sin\gamma + w_z \\ -\frac{C_D S\rho(z)}{2}\frac{V^2}{m} - g\sin\gamma + \frac{T}{m} \\ \frac{C_L S\rho(z)}{2}\frac{V}{m}\sin\phi \\ -\eta T \end{bmatrix}. \tag{1}$$

The states are the cartesian coordinates x and y, the altitude z, the true airspeed V (i.e., the speed of the aircraft relative to the surrounding air), the heading angle ψ, and the mass m. The aerodynamic lift and drag coefficients C_D and C_L, the surface area of the wings S, the fuel flow coefficient η, and the air density $\rho(h)$ are obtained from the base of aircraft data (BADA) [43]. Let $\begin{bmatrix} x_1 & x_2 & x_3 & x_4 & x_5 & x_6 \end{bmatrix}^T = \begin{bmatrix} x & y & z & V & \psi & m \end{bmatrix}^T$ denote the state variables and notice that the aircraft engine thrust T, the flight path angle γ, and the bank angle ϕ, represent the control inputs in the above set of equations, which, due to aerodynamic limitations, have to satisfy constraints of the form $\underline{T} \leq T \leq \overline{T}$, $\underline{\gamma} \leq \gamma \leq \overline{\gamma}$, $\underline{\varphi} \leq \varphi \leq \overline{\varphi}$. The wind speed vector is denoted by $\upsilon = \begin{bmatrix} w_x & w_y & w_z \end{bmatrix}^T \in \mathbb{R}^3$.

To ensure that the aircraft does not stray too far off its reference path in the $x-y$ coordinates, the bank angle ϕ is set based on the heading error and the cross track deviation of the aircraft from the reference path. In [47] and [48], a nonlinear controller was developed to emulate the lateral corrective actions of the aircraft flight management system. To counteract for a long track errors, we also implement here a time of arrival controller, as described in Section II-C.

The stochastic nature of the model developed in [47] and [48], enters through the wind component $\upsilon \in \mathbb{R}^3$. The wind, that an aircraft encounters, comprises a deterministic component, available through meteorological forecasts, and a stochastic wind prediction error. The wind prediction error, that an aircraft encounters, is correlated to the wind experienced by all other aircraft not only at a given time instance, but also at earlier and later times. By taking this into account, realistic weather scenarios can be generated as described in [47] and [48].

The flight management system determines the control input according to different discrete modes [43]. In the context of this paper, the main task of the FMS of each aircraft $j = 1, \ldots, N$, is to track the flight plan, which can be thought of as a sequence of way points. Way points are characterized by their 3-D coordinates

$$O_{(i,j)} = \begin{bmatrix} O^x_{(i,j)} & O^y_{(i,j)} & O^z_{(i,j)} \end{bmatrix}^T \in \mathbb{R}^3_+$$

where $i = 1, \ldots, M_j$. They define $M_j - 1$ straight line flight segments, and give rise to a discrete state i, which stores the segment of the flight that aircraft j is currently in. The decision making logic of the FMS also involves additional discrete states whose dynamics are expressed in terms of finite state machines. One example is the flight level, which is characterized by the altitude z, and determines the nominal airspeed of the aircraft V_{nom}. Additionally, the flight phase (cruise, climb, descent) determines the thrust input T, which is set accordingly, to track the nominal airspeed V_{nom}. Further discussion and a detailed description of these and other discrete modes of the FMS is given in [43].

B. From Way Points to TWs

TWs can be considered as space rectangles that each aircraft must hit within a specified time interval. Following the CATS concept of operations [6], we assume that the TWs are located on the boundary between air traffic control sectors, which

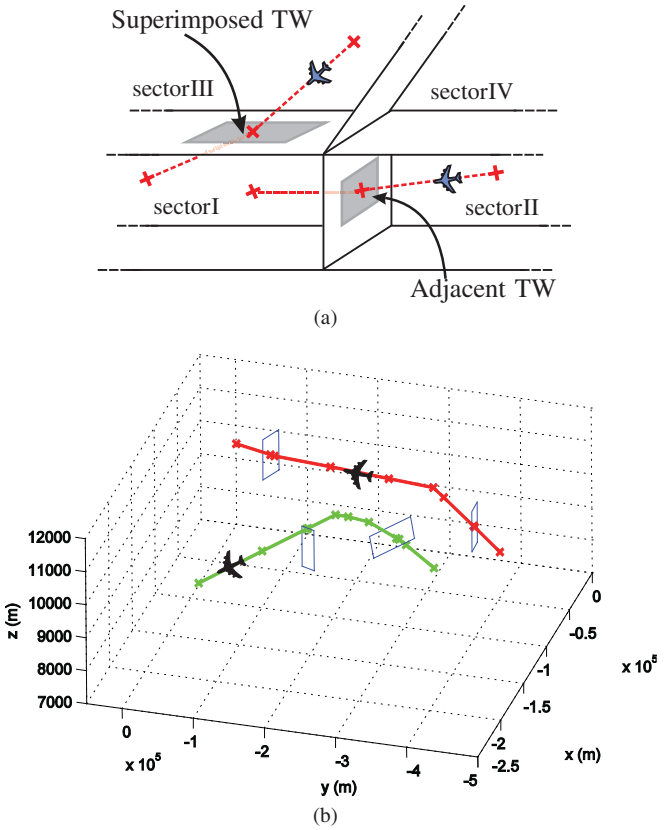

Fig. 1. (a) Superimposed and adjacent TWs placed at the borders between vertically and horizontally separated control sectors, respectively. (b) Two flights with their TWs. The first TW of the green flight is superimposed, whereas all the others are adjacent.

consist of airspace regions where a different control authority (i.e., air traffic controller) is responsible for the safe and efficient management of flights. If the sectors are superimposed vertically the TWs are called superimposed, otherwise they are called adjacent [Fig. 1(a)]. In Fig. 1(b) two sample flights with their TWs, from the CATS HIL experiments used in our validation simulations below, are depicted. Motivated by the procedures adopted for the CATS HIL simulations, we introduce two assumptions for the TW elements.

1) The center of every TW is always a waypoint in the flight plan.
2) TWs do not overlap in space and time.

C. TW Tracking Controller

A time of arrival controller was designed to regulate along track errors and enable the simulated aircraft to meet the timing constraints imposed by their TWs. Our design is inspired by [49] and [50], and can be found in detail in [51]. It aims to mimic the potential actions that air traffic controllers or pilots may take to track TWs in the simulation environment of Section II-A. As such, it should not be considered as an attempt to design a full scale 4-D FMS. Our choices are partly dictated by observations of air traffic controllers and pilots that took part in the CATS HIL experiments [8]. The output of the proposed control scheme is the sum of the nominal speed (determined by the flight level and retrieved from [43]) and a correction term $V_d(t) = V_{\text{nom}} + Ke$, where

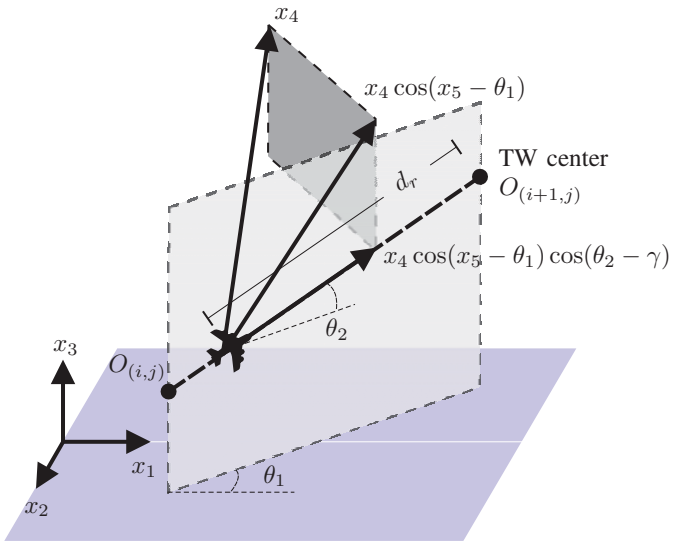

Fig. 2. Projection of speed x_4 along flight plan segment $O_{(i,j)} - O_{(i+1,j)}$. Variable d_r denotes the distance to the center of the next TW along flight plan.

e denotes the tracking error as a function of the continuous state vector of the system, as well as the wind information and the flight plan. Variable V_d represents the desired speed that the thrust command will try to track. For simplicity, in the computation of the tracking error, we assume that the current airspeed and wind speed is maintained constant throughout the remaining part of the flight path until the following TW. Similar assumptions hold also for the current wind speed value. The tracking error is then defined as

$$e = d_r - (t_d - t)\left(x_4 \cos(x_5 - \theta_1)\cos(\theta_2 - \gamma) + w_p\right) \quad (2)$$

where d_r denotes the distance to the center of the next TW along the flight plan, t_d is the desired time of arrival, which in this case was considered to be the middle of the TWs time interval, and K is a gain. The term $x_4 \cos(x_5 - \theta_1)\cos(\theta_2 - \gamma)$ is the projection of the speed x_4 along the flight plan (see Fig. 2), and θ_1 and θ_2 are defined as

$$\theta_1 = \tan^{-1}\left(\frac{O^y_{(i+1,j)} - x_2}{O^x_{(i+1,j)} - x_1}\right)$$

$$\theta_2 = \tan^{-1}\left(\frac{O^z_{(i+1,j)} - x_3}{\sqrt{\left(O^x_{(i+1,j)} - x_1\right)^2 + \left(O^y_{(i+1,j)} - x_2\right)^2}}\right).$$

The wind speed vector w_p is similarly defined as the projection of the wind speed vector along the flight plan.

III. Determining the Limits of Maneuverability Using Reachability

Our objective in this section is to determine, for each aircraft, the limits of maneuverability afforded due to the presence of TWs. To achieve this, we propose a reachability based methodology, which is based on computing the set of states from which an aircraft can start from and reach its TWs while avoiding conflict with other aircraft. We first

start by characterizing such reach-avoid problems, since they are the core of the algorithm proposed in Section III-C. For the implementation of this algorithm, we describe, at an intermediate step, how the detailed model of Section II can be abstracted to allow the use of reachability based numerical tools.

A. Reach-Avoid Problem Characterization

We first consider the case of static "avoid" sets, which encode state constraints that do not evolve with time. Motivated by [17], consider the continuous time system $\dot{x} = f(x,u,v)$, with $x \in \mathbb{R}^n$, $f(\cdot,\cdot,\cdot) : \mathbb{R}^n \times U \times V \to \mathbb{R}^n$, and $u \in U \subseteq \mathbb{R}^m$, $v \in V \subseteq \mathbb{R}^p$.[1] Let $\mathcal{U}_{[t,t']}$, $\mathcal{V}_{[t,t']}$ denote the set of Lebesgue measurable functions from the interval $[t,t']$ to U, and V, respectively, and let $T \geq 0$ to be an arbitrary time horizon. Also consider the functions $l(\cdot): \mathbb{R}^n \to \mathbb{R}$ and $h(\cdot): \mathbb{R}^n \to \mathbb{R}$, that will be used to characterize the "reach" and the "avoid" set, respectively.

Assumption 1: The sets $U \subseteq \mathbb{R}^m$ and $V \subseteq \mathbb{R}^p$ are compact. The functions $f(x,u,v)$, $l(x)$ and $h(x)$ are bounded, Lipschitz continuous in x, and continuous in u and v. Moreover, for all $x \in \mathbb{R}^n$, $\bigcup_{u\in U} f(x,u,v)$, $\bigcup_{v\in V} f(x,u,v)$ are compact and convex for all $v \in V$ and all $u \in U$, respectively.

For $t \in [0,T]$, $u(\cdot) \in \mathcal{U}_{[t,T]}$ and $v(\cdot) \in \mathcal{V}_{[t,T]}$, let $\phi(\cdot,t,x,u(\cdot),v(\cdot)): [t,T] \to \mathbb{R}^n$ denote the system trajectory, which under Assumption 1, is unique for each initial state x. The last part of Assumption 1 ensures the existence of an optimal control trajectory, and is only needed to show that the reachable sets are closed. Following [36], [52], we restrict the first player to play nonanticipative strategies. A nonanticipative strategy is a function $\alpha : \mathcal{V}_{[0,T]} \to \mathcal{U}_{[0,T]}$ such that for all $s \in [t,T]$ and for all $v, \hat{v} \in \mathcal{V}$, if $v(\tau) = \hat{v}(\tau)$ for almost every $\tau \in [t,s]$, then $\alpha[v](\tau) = \alpha[\hat{v}](\tau)$ for almost every $\tau \in [t,s]$. We then use $\mathcal{A}_{[t,T]}$ to denote the class of nonanticipative strategies.

Consider a closed set R (the "reach" set), and an open set A (the "avoid" set). Following [17], we relate them to the level sets of the Lipschitz continuous functions $l(\cdot): \mathbb{R}^n \to \mathbb{R}$ and $h(\cdot): \mathbb{R}^n \to \mathbb{R}$, i.e., $R = \{x \in \mathbb{R}^n \mid l(x) \leq 0\}$ and $A = \{x \in \mathbb{R}^n \mid h(x) > 0\}$. As in [17], we list two reach-avoid problems of interest that will be used in the reachability calculations of Section III-C.

1) Reach-Avoid at the Terminal Time: We first determine the set of initial states $RA(t,R,A)$ for which there exists a choice for the control inputs such that, for any disturbance, the system trajectories reach the set R exactly at the terminal time T, without passing through the set A over the time horizon $[t,T]$, as follows:

$$RA(t,R,A) = \Big\{x \in \mathbb{R}^n \mid \exists \alpha(\cdot) \in \mathcal{A}_{[t,T]}, \quad \forall v(\cdot) \in \mathcal{V}_{[t,T]}, \\ (\phi(T,t,x,\alpha(\cdot),v(\cdot)) \in R) \wedge (\forall \tau \in [t,T], \\ \phi(\tau,t,x,\alpha(\cdot),v(\cdot)) \notin A)\Big\}. \tag{3}$$

[1]Note that x in this case is the state vector and should not be related to the cartesian coordinate defined in the previous section. Throughout this paper, it will always be clear from the context to which x we refer.

In [17], the value function $V: \mathbb{R}^n \times [0,T] \to \mathbb{R}$ was introduced as

$$V(x,t) = \inf_{\alpha(\cdot)\in\mathcal{A}_{[t,T]}} \sup_{v(\cdot)\in\mathcal{V}_{[t,T]}} \max\{l(\phi(T,t,x,\alpha(\cdot),v(\cdot))), \\ \max_{\tau\in[t,T]} h(\phi(\tau,t,x,\alpha(\cdot),v(\cdot)))\}. \tag{4}$$

It was shown that $RA(t,R,A) = \{x \in \mathbb{R}^n \mid V(x,t) \leq 0\}$, and was then proven that $V(x,t)$ is the unique continuous viscosity solution of the quasi-variational inequality

$$\max\{h(x) - V(x,t), \frac{\partial V}{\partial t}(x,t) \\ + \sup_{v\in V} \inf_{u\in U} \frac{\partial V}{\partial x}(x,t) f(x,u,v)\} = 0 \tag{5}$$

with terminal condition $V(x,T) = \max\{l(x), h(x)\}$.

2) Reach-Avoid at Any Time: In addition, we also need to characterize the set of initial states $\widetilde{RA}(t,R,A)$ from which there exists a choice for the control input such that, for any disturbance, the trajectories of the system reach the set R at some time within the time horizon $[t,T]$ (not necessarily at the terminal time), without passing through the set A prior to hitting R

$$\widetilde{RA}(t,R,A) = \Big\{x \in \mathbb{R}^n \exists \alpha(\cdot) \in \mathcal{A}_{[t,T]}, \forall v(\cdot) \in \mathcal{V}_{[t,T]}, \exists \tau_1 \\ \in [t,T], (\phi(\tau_1,t,x,\alpha(\cdot),v(\cdot)) \in R) \wedge \\ (\forall \tau_2 \in [t,\tau_1], \phi(\tau_2,t,x,\alpha(\cdot),v(\cdot)) \notin A)\Big\}. \tag{6}$$

To characterize this set, in [17] it was shown that for all $t \in [0,T]$, $\widetilde{RA}(t,R,A) = \{x \in \mathbb{R}^n \mid \widetilde{V}(x,t) \leq 0\}$, where

$$\widetilde{V}(x,t) = \inf_{\alpha(\cdot)\in\mathcal{A}_{[t,T]}} \sup_{v(\cdot)\in\mathcal{V}_{[t,T]}} \min_{\tau_1\in[t,T]} \\ \max\Big\{l(\phi(\tau_1,t,x,\alpha(\cdot),v(\cdot))), \\ \max_{\tau_2\in[t,\tau_1]} h(\phi(\tau_2,t,x,\alpha(\cdot),v(\cdot)))\Big\}.$$

The value function $\widetilde{V}(x,t)$ was proven in [17] to be the unique continuous viscosity solution of the quasi-variational inequality

$$\max\Big\{h(x) - V(x,t), \frac{\partial V}{\partial t}(x,t) \\ + \min\Big\{0, \sup_{v\in V} \inf_{u\in U} \frac{\partial V}{\partial x}(x,t) f(x,u,v)\Big\}\Big\} = 0 \tag{7}$$

with terminal condition $V(x,T) = \max\{l(x), h(x)\}$.

To solve (5) and (7) numerically, and enforce the constraint encoded by $h(\cdot)$ on $V(x,t)$ and $\widetilde{V}(x,t)$, one could either use tools for solving variational inequalities [32], or standard tools based on level set methods [39]. In both cases, a procedure known as masking [53] is used.

3) Extension to Time-Dependent State Constraints: The reach-avoid framework defined so far considers only static "avoid" sets characterized by a function $h(\cdot): \mathbb{R}^n \to \mathbb{R}$. In general, extension to time-dependant state constraints requires the following procedure outlined in [54]. For the specific problem, where the TWs impose a fixed temporal constraint at the end of each flight segment, such an extension is straightforward. For the sake of completeness, we describe

how time-dependant state constraints can be captured, for general, the class of target hitting problems. Similar to [54], for $t \in [0, T]$ consider the time-dependent "avoid" set $A_t \subseteq \mathbb{R}^n$, where A_t characterizes the region of the state space, through which system trajectories should not pass at time t. We can now augment the state equations with a timer $\bar{x}$, and define the new state vector $\tilde{x} = (x, \bar{x}) \in \mathbb{R}^{n+1}$ with $\tilde{f} = (f, 1) \in \mathbb{R}^{n+1}$. In the augmented space, the "avoid" region can be defined as

$$A = \bigcup_{t \in [0,T]} A_t \times \{t\}$$

allowing us to use the formulation of the previous sections, with $\tilde{x}$ in place of x, and $h(\cdot)\colon \mathbb{R}^{n+1} \to \mathbb{R}$ to characterize A. Note that $\tilde{x} \notin A$ is equivalent to $x(t) \notin A_t$ for all $t \in [0, T]$.

In the formulation of Section III-C, the "avoid" region encodes the set of states for each aircraft that might be in conflict with other aircraft, and therefore it is time dependent. Hence, for the rest of this paper, we will use $h(x, t)$ to make this dependency explicit.

B. Model Abstraction

The aircraft and FMS model described so far is adequate for simulation purposes, but it is computationally expensive to analyze. Most of the reachability numerical methods are based on gridding the state space, so the memory and time necessary for the computation grow exponentially in the state dimension. Therefore, using a full six-state point mass model of the aircraft, like the one described in Section II-A, would not be feasible. To make the reachability computations tractable, we perform a series of simplifications.

1) We eliminate the speed equation from (1), and use V as a control input. Using aircraft parameter values for an airbus A330 cruising at 35 000 ft (taken from [43]), an aircraft would need ∼16 s to change from the minimum to the maximum value of the considered speed envelope (±10% of the nominal one) under full thrust. In this time, it would cover a distance of less than 2 km, which is relatively small compared to the time scale (∼25 minutes) and distances (∼350 km) of the reachability calculations. This observation is also supported by a study into the time scale separation of flight dynamics [23], where speed is used as control variable in reachability calculations involving position variables (albeit for a different class of flight vehicles with very similar dynamics). In specific cases, however, where the outcome of the reachability calculations needs to be refined, we could apply our methodology without performing this simplification.
2) We assume that the aircraft perfectly tracks the flight plan laterally. This is not unreasonable since cross-track errors are, in general, much smaller than along-track errors [13]; indeed, modern aircraft with an advanced flight management system laterally track their flight plan to within ±1 nmi for 95% of the time [55].[2]

[2]Note that 1 nmi = 1852 m and 1 ft = 0.305 m.

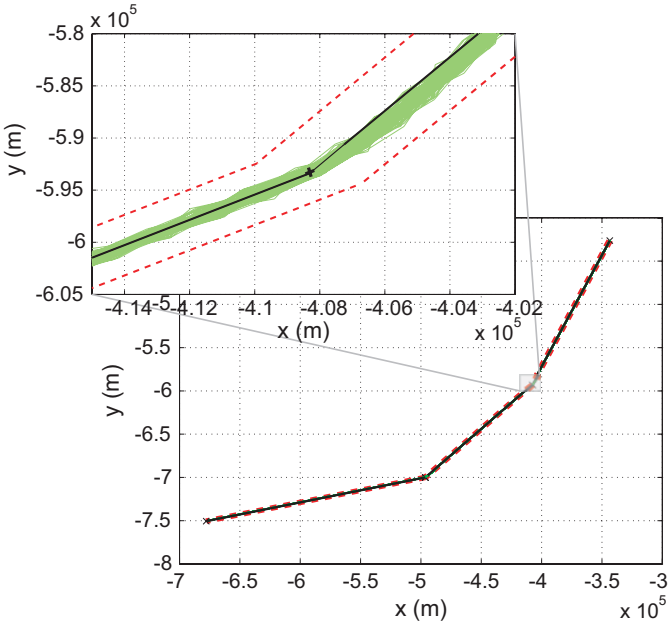

Fig. 3. Flight track projections on the x–y axis for one of the flights of Fig. 11, for 1000 different uncertainty realizations (wind, mass, and entry time uncertainty, as defined in Section IV-A). The black line is the flight plan, whereas the red dotted lines correspond to ±1 nmi required navigation performance values.

For the simulation model outlined in Section II, this is also justified by inspection of Fig. 3, which shows a segment of 1000 simulated trajectories for one of the flights of Fig. 11, corresponding to different uncertainty realizations, as these will be defined in the next section (±1 nmi lateral accuracy [55]).

In the notation of [31], the dynamics of aircraft j can be modeled by a hybrid automaton $H_j = (X_j, Q_j, \text{Init}_j, f_j, \text{Dom}_j, G_j, R_j)$, with the following.

1) Continuous states: $x_j = \begin{bmatrix} s_j & z_j & t \end{bmatrix}^T \in \mathbb{R}^3_+ = X_j$.
2) Discrete states: $i \in \{0, ..., M_j - 1\} = Q_j$.
3) Initial states: $\text{Init}_j = \{(i, s_j, z_j, t) \mid i = 0, s_j = 0, z_j = z_{j_0}\}$.
4) Control inputs: $u_j = \begin{bmatrix} b_j & \gamma_j \end{bmatrix}^T \in [-1, 1] \times \left[-\overline{\gamma_j}, \overline{\gamma_j}\right] = U_j$.
5) Disturbance inputs: $v = \begin{bmatrix} w_x & w_y & w_z \end{bmatrix}^T \in V \subseteq \mathbb{R}^3$.
6) Vector field: $f_j : Q_j \times X_j \times U_j \times V \to X_j$

$$f_j(i, s_j, z_j, t, u_j, v) = \begin{bmatrix} \dot{s}_j \\ \dot{z}_j \\ \dot{t} \end{bmatrix}$$

where $\dot{s}_j = (1+0.1b_j)g(z_j, \gamma_j)\cos\gamma_j + w_x \cos\Psi_{(i,j)} + w_y \sin\Psi_{(i,j)}$, $\dot{z}_j = (1+0.1b_j)g(z_j, \gamma_j)\sin\gamma_j + w_z$ and $\dot{t} = 1$.
7) Domain: $\text{Dom}_j = \{(i, s_j, z_j, t) \mid s_j \le d_{(i,j)}\}$.
8) Guards: $G_j(i, i+1) = \{(s_j, z_j, t) \mid s_j \ge d_{(i,j)}\}$.
9) Reset map: $R_j(i, i+1, s_j, z_j, t) = \{(0, z_j, t)\}$.

The schematic diagram of Fig. 4 illustrates the modes of the hybrid automaton for the simplified aircraft model.

For each aircraft j, $\Psi_{(i,j)}$ denotes the angle that the segment i forms with the x axis, and $\Gamma_{(i,j)}$ the flight path

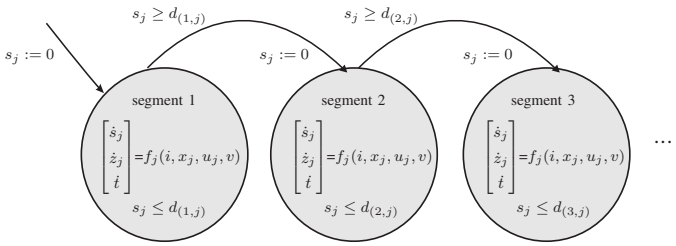

Fig. 4. Hybrid automaton for the simplified aircraft model. Each discrete mode corresponds to the flight segment that the aircraft is currently in.

angle that it forms with the horizontal plane (Fig. 5). For $i = 1, \ldots, M_j - 1$, we can define

$$\Psi_{(i,j)} = \tan^{-1}\left(\frac{O^y_{(i+1,j)} - O^y_{(i,j)}}{O^x_{(i+1,j)} - O^x_{(i,j)}}\right)$$
$$\Gamma_{(i,j)} = \tan^{-1}\left(\frac{O^z_{(i+1,j)} - O^z_{(i,j)}}{d_{(i,j)}}\right)$$

where $d_{(i,j)} = \sqrt{(O^x_{(i+1,j)} - O^x_{(i,j)})^2 + (O^y_{(i+1,j)} - O^y_{(i,j)})^2}$ is the length of the projection of segment i on the horizontal plane. Since we assume that lateral tracking is perfect, it suffices to track the distance of each segment covered on the horizontal plane, denoted by $s_j \in \mathbb{R}_+$ in Fig. 5. The cartesian coordinates can be then computed by

$$\begin{bmatrix} x_{(i,j)}(s_j) \\ y_{(i,j)}(s_j) \end{bmatrix} = \begin{bmatrix} O^x_{(i,j)} \\ O^y_{(i,j)} \end{bmatrix} + \begin{bmatrix} \cos\Psi_{(i,j)} \\ \sin\Psi_{(i,j)} \end{bmatrix} s_j.$$

To approximate accurately the physical model, the flight path angle γ_j is fixed according to the angle $\Gamma_{(i,j)}$ that the segment forms with the horizontal plane. If $\Gamma_{(i,j)} = 0$ the aircraft will be cruising ($\gamma_j = 0$) at that segment, whereas if it is positive or negative it will be climbing ($\gamma_j \in [0, \overline{\gamma}_j]$) or descending ($\gamma_j \in [-\overline{\gamma}_j, 0]$), respectively.

As discussed in Section II-A, the nominal airspeed of the aircraft depends on the flight level and whether the aircraft is climbing, cruising, or descending. We approximate this dependence by a linear interpolation of the speed-altitude values of [43], denoted by the function $g(z_j, \gamma_j)$. In general, aircraft fly faster at higher altitudes, hence $g(\cdot, \gamma_j)$ is a nondecreasing function. For our simulations, assume that the actual airspeed (treated as a control input in the simplified model) is allowed to vary within $\pm 10\%$ of the nominal one; this is reflected by the control input $b_j \in [-1, 1]$.

Apart from s_j, the other two continuous states are the altitude z_j and the time t. The last equation was included in order to track the TW temporal constraints. As already stated, the wind speed v is assumed to act as a bounded disturbance with $-\overline{v} \leq v \leq \overline{v}$. For our simulations, we considered $\overline{v} = 12$ m/s, corresponding to 3σ of the values in [46]. Since the flight path angle γ_j does not exceed 5°, for simplicity, we can assume that $\sin\gamma_j \approx \gamma_j$ and $\cos\gamma_j \approx 1$.

The constraint set for each aircraft j (corresponding to the TW located at $O_{(i,j)}$) can be then defined as $K_j = (d_{(i,j)}, [z_{(i,j)} + \underline{z}_{(i,j)}, z_{(i,j)} + \overline{z}_{(i,j)}], [\underline{t}_j, \overline{t}_j])$ if the TW is adjacent ($\underline{z}_{(i,j)}, \overline{z}_{(i,j)}$ denote the extremities of the TW in the vertical direction), and $K_j = ([d_{(i,j)} + \underline{s}_{(i,j)}, d_{(i,j)} + \overline{s}_{(i,j)}], z_{(i,j)}, [\underline{t}_j, \overline{t}_j])$ if the TW is superimposed ($\underline{s}_{(i,j)}, \overline{s}_{(i,j)}$ denote the extremities of the TW along the s direction). By $\underline{t}_j$ and $\overline{t}_j$, we denote the temporal extremities of the TWs. Note that using this abstracted version of the model, TWs are represented as line segments. This is used only for the reachability calculations of Section IV-C, whereas for the Monte Carlo analysis of Section IV-B and the CATS HIL experiments, the initial TW representation is employed.

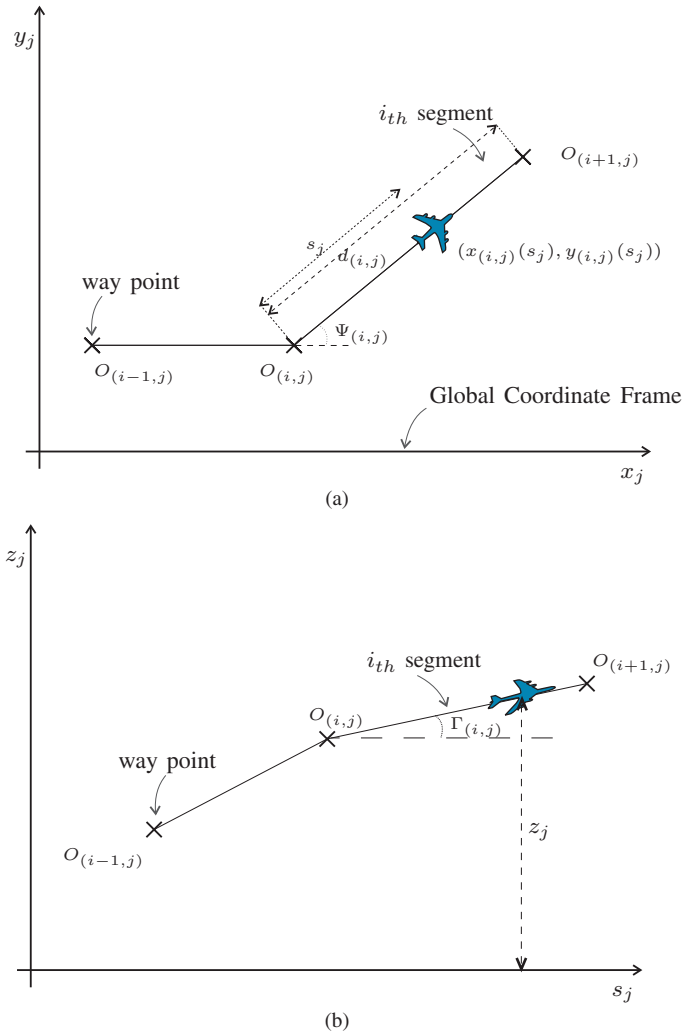

Fig. 5. (a) Flight plan projection on the horizontal plane. The aircraft does not deviate from the nominal flight plan due to the simplifying assumption of constant heading angle at each segment. (b) Flight plan projection on the z-s plane.

C. Reach-Avoid Tubes for TW Tracking and Conflict Avoidance

In air traffic, conflict refers to the loss of minimum separation between two aircrafts. Each aircraft is surrounded by a protected zone, which is generally considered as a cylinder of radius 5 nmi and height 2000 ft centered at the aircraft. If this zone is violated by another aircraft then a conflict is said to have occurred.

We now show how the problem of meeting TW constraints while avoiding conflicts can be formulated as a reach-avoid

problem. Note that, even though the simplified model is strictly speaking hybrid, the discrete modes are visited sequentially. Hence, we can perform a sequential calculation involving only the continuous dynamics, treating the initial set computed for each flight plan segment as the terminal condition for the previous segment. In the opposite case, the assumptions and algorithm proposed in [31] should be followed instead. For the rest of this paper, we will refer to the computed sets as reachable tubes.[3] Similar to the definition of the set K_j, we define, for each aircraft j, the spatial constraints of a TW centered at the way point $O_{(i,j)}$ as $\widetilde{R}_j = (d_{(i,j)}, [z_{(i,j)} + \underline{z}_{(i,j)}, z_{(i,j)} + \overline{z}_{(i,j)}])$ if the TW is adjacent, and $\widetilde{R}_j = ([d_{(i,j)} + \underline{s}_{(i,j)}, d_{(i,j)} + \overline{s}_{(i,j)}], z_{(i,j)})$ if the TW is superimposed. Let also $[\underline{t}_j, \overline{t}_j]$ denote the temporal extent of $\widetilde{R}_j$.

Stage 0: For each aircraft j, apply the procedure outlined in Stage 1 and 2 without "avoid" regions. Thus, we can compute the reachable tubes for each aircraft and identify for every time instance the states that correspond to conflicting situations. Specifically, for $t \in [\underline{t}_j, \overline{t}_j]$, let $\widetilde{A}_{ji,t}$ denote all states x_j for which the aircraft j is in conflict with another aircraft $i \neq j$ at time t, and use $h_{ji}(x_j, t)$ to characterize this set. We can then define the obstacle function $h_j(x_j, t) = \max_{i \neq j} h_{ji}(x_j, t)$ to characterize the "avoid" region $\widetilde{A}_{j,t} = \bigcup_{i \neq j} \widetilde{A}_{ji,t}$, capturing the case of multiple conflicts. Similar calculations for $t \leq \underline{t}_j$ give rise to the "avoid" region $A_{j,t}$. Note that by defining any region of conflict as an "avoid" set for all involved aircraft may be conservative; if an automated conflict resolution procedure is employed the conservatism of the resulting solution may be reduced.

Stage 1: Compute for each aircraft j, the set R_j of states x_j at time $\underline{t}_j$ (beginning of TW) from which there exists a nonanticipative strategy for the control input that for all wind realizations can lead the aircraft inside $\widetilde{R}_j$ at least once within the time interval $[\underline{t}_j, \overline{t}_j]$, while avoiding conflict with other aircraft. This is a reach-avoid at any time calculation. The corresponding set $\widetilde{RA}_j(\underline{t}, \widetilde{R}_j, \widetilde{A}_{j,t})$ is the zero sublevel set of $\widetilde{V}$, which is the solution of

$$\max\left\{h_j(x_j,t) - \widetilde{V}(x_j,t), \frac{\partial \widetilde{V}}{\partial t}(x_j,t) + \min\left\{0, H_{ij}(p,x_j)\right\}\right\} = 0$$

where

$$H_{ij}(p,x) = \sup_{v \in V} \inf_{u_j \in U_j} \Big(p_1(1+0.1b_j)g(z_j,\gamma_j) + p_2(1+0.1b_j) \times g(z_j,\gamma_j)\gamma_j + p_1 \cos\Psi_{(i,j)} w_x + p_1 \times \sin\Psi_{(i,j)} w_y + p_2 w_z \Big)$$

is the Hamiltonian of the system, with $u_j = \begin{bmatrix} b_j & \gamma_j \end{bmatrix}^T$ and $v = \begin{bmatrix} w_x & w_y & w_z \end{bmatrix}^T$. Since TWs do not overlap, the terminal condition is $\widetilde{V}(x_j, \overline{t}_j) = l_j(x_j)$. The function $l_j(\cdot)$ can be set equal to the signed distance to the set $\widetilde{R}_j^c$

$$l(x_j) = \begin{cases} \inf_{\hat{x}_j \in \widetilde{R}_j} |x_j - \hat{x}_j|, & \text{if } x_j \in \widetilde{R}_j^c \\ -\inf_{\hat{x}_j \in \widetilde{R}_j} |x_j - \hat{x}_j|, & \text{if } x_j \in \widetilde{R}_j. \end{cases}$$

Similarly, $h_j(\cdot, t)$ is defined to be the signed distance to the set $\widetilde{A}_{j,t}$ that was computed at Stage 0. The functions $l_j(\cdot)$ and $h_j(\cdot, t)$ are Lipschitz by construction; to ensure that they are bounded and satisfy Assumption 1, we saturate them at their Lipschitz constants by setting them equal to their Lipschitz constant wherever they are greater than this value and minus the Lipschitz constant wherever they are less than this value. For the numerical implementation, this is not an issue since the computations are performed over compact sets.

Stage 2: Compute for each aircraft j, the set of all states at time $t \leq \underline{t}_j$ for which there exists a nonanticipative strategy for the control input such that for all wind realizations the system can reach the set R_j (determined at Stage 1) at time $\underline{t}_j$, while avoiding conflict with other aircraft. Based on the analysis of Section III-A, this is a reach-avoid at the terminal time set $RA_j(t, R_j, A_{j,t})$, and can be computed by solving

$$\max\left\{h_j(x_j,t) - V(x_j,t), \frac{\partial V}{\partial t}(x_j,t) + H_{ij}(p,x_j)\right\} = 0$$

with $V(x_j, \underline{t}_j) = \max\{\widetilde{V}(x_j, \underline{t}_j), h_j(x_j, t)\}$. Based on the computation of Stage 1, the set $R_j = \{x_j \in \mathbb{R}^n | \ \widetilde{V}(x_j, \underline{t}_j)) \leq 0\}$, whereas $A_{j,t}$ depends once again on the obstacle function $h_j(x_j, t)$, and is defined similar to $\widetilde{A}_{j,t}$.

The optimal control and disturbance inputs needed in the calculation can be analytically computed by inspecting the Hamiltonian of the system for each segment i. The optimal value for w_x is therefore given by

$$w_x^* = \begin{cases} \overline{w}_x & \text{if } p_1 \cos\Psi_{(i,j)} \geq 0 \\ -\overline{w}_x & \text{if } p_1 \cos\Psi_{(i,j)} < 0. \end{cases}$$

In a similar way, we can define w_y^* and w_z^*. Likewise, and since $(1 + 0.1b_j)g(z_j, \gamma_j) > 0$, we have

$$\gamma_j^* = \begin{cases} \overline{\gamma}_j & \text{if } (p_2 \leq 0 \wedge \Gamma_{(i,j)} > 0) \\ 0 & \text{if } (p_2 > 0 \wedge \Gamma_{(i,j)} > 0) \\ & \vee (p_2 \leq 0 \wedge \Gamma_{(i,j)} < 0) \\ -\overline{\gamma}_j & \text{if } (p_2 > 0 \wedge \Gamma_{(i,j)} < 0) \end{cases}$$

$$b_j^* = \begin{cases} 1 & \text{if } p_1 + p_2\gamma_j^* \leq 0 \\ -1 & \text{if } p_1 + p_2\gamma_j^* > 0. \end{cases}$$

For the case where $\Gamma_{(i,j)} = 0$ (cruising), $b_j^* = 1$ if $p_1 \leq 0$ and $b_j^* = -1$ if $p_1 > 0$. Note that the resulting control inputs are not only nonanticipative, but also feedback, since they depend only on the state of the system via the costate vector $p = \partial V / \partial x_j$.

The steps of the reach-avoid computation for each aircraft j are summarized in Algorithm 1. In Section IV-D, we will show how this method can be used to advise air traffic controllers whether the introduction of an additional TW (e.g., in case of conflict), changing the flight plan laterally and longitudinally, is safe and feasible with respect to the existing TW sequence.

[3]Using the terminology of [56], the outcome of the first stage of the proposed methodology should be referred to as reachable tubes, whereas the outcome of the second stage should be referred to as reachable sets.

Algorithm 1 Reach-Avoid Computation for Each Aircraft j

Let $[\underline{t}_j, \overline{t}_j]$ denote the TW temporal constraints of aircraft j,
Stage 0. ▷ Solve from $t = \overline{t}_j$ until the previous TW:
  for $t \in [\underline{t}_j\ \overline{t}_j]$
    Solve $\frac{\partial \widetilde{V}}{\partial t}(x_j, t) + \min\{0, \sup_{v \in V} \inf_{u_j \in U_j} \frac{\partial \widetilde{V}}{\partial x_j}(x_j, t) f_j(x_j, u_j, v)\} = 0,$
    with boundary condition $\widetilde{V}(x_j, \overline{t}_j) = l(x_j)$,
    ▷ it was assumed that TW do not overlap
    for $i \neq j$
      $C_{ji} = \{x_j \mid i, j$ are in conflict at time t$\}$,
      Define $h_{ji}(x_j, t)$: $\widetilde{A}_{ji,t} = \{x_j \mid h_{ji}(x_j, t) > 0\} \supseteq C_{ji}$ is the smallest box containing C_{ji}.
    end for
    if $\widetilde{A}_{j,t} = \bigcup_{i \neq j} \widetilde{A}_{ji,t} \neq \emptyset$ ▷ multiple conflicts.
      $h_j(x_j, t) = \max_{i \neq j} h_{ji}(x_j, t)$, ▷ characterizes $\widetilde{A}_{j,t}$.
    end if
  end for
  for $t \leq \underline{t}_j$
    Solve $\frac{\partial V}{\partial t}(x_j, t) + \sup_{v \in V} \inf_{u_j \in U_j} \frac{\partial V}{\partial x_j}(x_j, t) f_j(x_j, u_j, v) = 0,$
    with boundary condition $V(x_j, \underline{t}_j) = \widetilde{V}(x_j, t)$.
    Repeat steps $6 - 12$ and compute $A_{j,t}$.
  end for
Stage 1. ▷ For $t \in [\underline{t}_j\ \overline{t}_j]$ repeat steps $4 - 5$ and compute $\widetilde{V}(x_j, t)$.
  if $\widetilde{A}_{j,t} \neq \emptyset$
    $\widetilde{V}(x_j, t) = \max(h_j(x_j, t), \widetilde{V}(x_j, t))$.
    ▷ performs the masking operation of Section III-A.
  end if
Stage 2. ▷ For $t \leq \underline{t}_j$ repeat steps $15 - 16$ and compute $V(x_j, t)$.
  Repeat steps $20 - 22$ with V instead of $\widetilde{V}$ and avoid region $A_{j,t}$.

IV. Simulation Results

A. Simulation Set-Up

We consider 50 flights with 117 TWs whose mean temporal size is ~ 7 minutes, extracted from the HIL experiments conducted within the CATS project [8]. The HIL experiments concentrated on the interface between the Geneva and Milan control centers. Each of the flights used comes with a flight plan, coordinates for the TW extremities, and the time width of each TW. For illustrative purposes, Fig. 6 gives an overview of the simulated flights and the geographical area of interest.

In [9], no time of arrival controller was used, whereas the following four different sources of uncertainty are considered and their effect on the TW size and the probability of conflict was analyzed by means of Monte Carlo simulations.

1) Wind uncertainty: We used the weather forecast error statistics of [57], as encoded for simulation in [47] and [48].
2) Aircraft mass uncertainty: We assumed a Gaussian distribution, with mean equal to the nominal aircraft mass m_{nom} provided by BADA [43] and standard deviation $\sigma = \min\{m_{\max} - m_{\text{nom}}, m_{\text{nom}} - m_{\min}\}/3$. All samples outside the minimum and maximum value of the aircraft mass ($m_{\min}$ and $m_{\max}$, respectively, based on BADA) were discarded.
3) Entry time uncertainty: We considered a uniform distribution between ± 1 minute from the center of the temporal interval of each aircraft's entry TW. Note that the range of values for the entry time uncertainty is less than the width of many TWs, to take implicitly into account the effect of speed adjustments by the air traffic controllers.
4) Nominal speed uncertainty: We assumed a uniform distribution between $\pm 6\%$ of the nominal speed value (not the actual one as in Section III-B), provided by BADA [43]. This range of values was dictated by the air traffic controllers that participated in the CATS HIL experiments. The extracted value was kept constant for every minute, and then a new sample was generated. It provides a naïve way of representing speed adjustments that air traffic controllers and/or pilots might perform. Subsequently, this source of uncertainty will be replaced by the more sophisticated time of arrival controller of Section II-C.

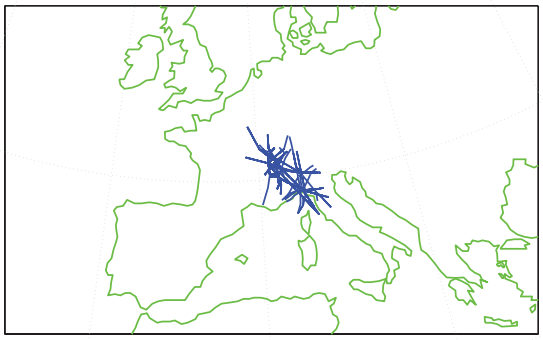

Fig. 6. Flight plan overview in the simulated airspace of the 50 simulated flights extracted from the HIL experiments.

The analysis of [9] implies that uncertainty in the wind and at the time, an aircraft enters the controlled sector plays a major role both in the TW hitting and the conflict probability. If wind is the only uncertainty source, its effect on the TW hitting probability distribution is still major, since the outcome of our simulation-based study would differ significantly from the deterministic case. Nevertheless, our results suggest that if wind is the only uncertainty source, the TWs used for the CATS HIL experiments [8] are rather conservative, as in many cases their size can be significantly reduced without a negative impact on the probability of meeting the TW constraints. This is not the case though when there is uncertainty on the time an aircraft enters the controlled sector, where more generous TW values are needed. This is reasonable, since an initial time deviation may lead to accumulate time errors, and hence the aircraft might violate subsequent TW constraints. This motivates the use of a time of arrival controller bellow, to avoid accumulating temporal deviations when moving from one TW to the next.

Motivated by these results, we concentrate on the case where both wind, mass, and entry time uncertainty is present, taking into account the two most important sources of uncertainty. In Section IV-B, we investigate the effect that the use of a time of arrival controller might have on the TW size and the probability of meeting the TW requirements. Finally, for the same scenario and for the flights that were found to be in conflict with high probability, in Section IV-C we apply the proposed reachability based algorithm to assess the limits of maneuverability that can be exploited to resolve the

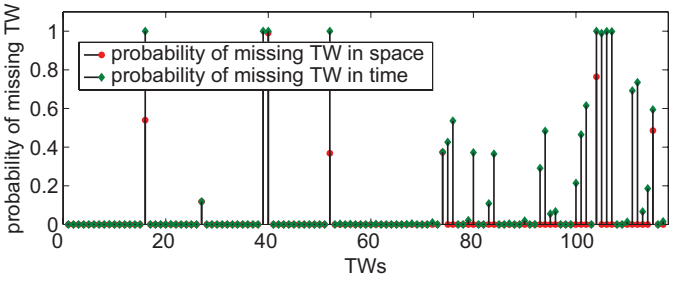

Fig. 7. Probability of missing each TW in space (red dots) and time (green diamonds). The results are based on 1000 Monte Carlo simulations corresponding to different uncertainty realizations (wind, mass, and entry time uncertainty); they are always more likely to violate the temporal instead of the spatial requirements of each TW. The flights are sorted based on their departure time, and, for each flight, TWs are listed according to the sequence in which they occur. The red dots indicate the probability of violating the spatial requirements of the TW constraints, whereas the green diamonds indicate the probability of missing a TW in time.

conflict while preserving the existing TW requirements. To illustrate how the algorithms developed here could be used for conflict resolution, we select by hand additional TWs within the maneuverability limits and demonstrate using Monte Carlo simulation that they indeed resolve the conflicts.

B. Impact of the Time of Arrival Controller on the TW Size

Considering wind, mass, and entry time uncertainty, and in the absence of time of arrival control, we attempt first to identify the probability of missing a TW in space and time, using 1000 Monte Carlo simulations for the 117 TWs of the simulated flights (Fig. 7). Fig. 7 shows that it is always more likely to violate the temporal, instead of the spatial, constraints of the TWs (some TWs are almost always missed in time). This is mainly due to the fact that TWs were designed for the HIL experiments and are rather generous in space [6] to leave enough maneuvering freedom to air traffic controllers in case they need to issue resolution maneuvers.

In view of determining the effect of the time of arrival controller on TW hitting probability and the TW size (mainly the temporal component due to the implications of Fig. 7), Fig. 8(a) and (b) correspond to the uncontrolled case, whereas Fig. 8(a) and (d) shows the results when the time of arrival controller was used. Each bar in Fig. 8(a) and (c) corresponds to a different TW time width (as a percentage of the nominal one), and its height indicates the corresponding TW hitting probability. Note that all TWs were reduced by the same fraction, shown on the horizontal axis of Fig. 8(a) and (c). In both cases, the probability of meeting the TW requirements is decreasing as we reduce the TW width. From a comparison though between Fig. 8(a) and 8(c), it is clear that by using a time of arrival controller we can achieve a very high TW hitting probability, even if we reduce the TWs time width to 50% of its initial value. This was not the case though in the uncontrolled scenario [Fig. 8(a)], where a significant reduction in the TW hitting probabilities was obtained. Note that the TWs time width is an indication though of how predictable a flight is; very tight intervals increase predictability on the one hand, but lead to smaller reachability envelopes on the other hand (less maneuverability).

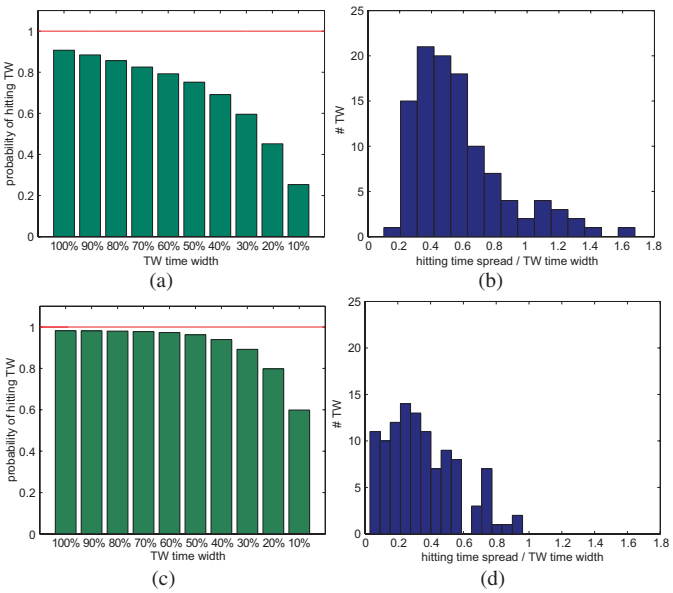

Fig. 8. (a) TW hitting probability with wind, mass, and entry time uncertainty, with all TWs reduced to a percentage of their original temporal size without time of arrival control. (b) TW size indicator with wind, mass, and entry time uncertainty, and without time of arrival control. (c) TW hitting probability with wind, mass, and entry time uncertainty, with all TWs reduced to a percentage of their original temporal size, using time of arrival control. (d) TW size indicator with wind, mass, and entry time uncertainty, using time of arrival control.

This is also implied by the distributions of Fig. 8(b) and (d), which show the TW size indicator. This is defined as the ratio of the spread of the TW hitting time distributions over the time width of each TW, and hence gives an indication of what the potential temporal size of the TW can be. The lower this value, the more the width of the TW can be reduced. In the case where a time of arrival controller is used, this ratio shifts to lower values [Fig. 8(d) compared to Fig. 8(b)], so the time width of the TWs can be reduced significantly. The spread of the TW hitting time distribution was calculated as the difference between the extreme TW hitting times, whereas to avoid outliers, the distribution could have been truncated at certain values. Note that a TW size indicator value less than one does not necessarily imply that the probability of missing this TW is zero. It could be the case that the TW hitting distribution is not contained in the TW (hence the TW hitting probability is less than one), but its spread is less than the TW's time width (TW size indicator less than one). In such cases, the corresponding TWs should be shortened and also shifted in time. For a better understanding, Fig. 9 illustrates the minimum and maximum TW hitting times (denoted by the extremities of the blue and red bars, respectively) relative to the TW center. Specifically, the average reduction in the TW hitting time spread is $\sim$1.41 minutes and the standard deviation is $\sigma = 1.04$ (the minimum and maximum reduction was 0.08 and 7.37 minutes, respectively). Note that the width of the region where the TWs overlap with the spread of the blue (red) bars (as a percentage of the TWs time width), does not necessarily indicate the probability of hitting the TWs in time, as this is shown in Fig. 7. This is due to the fact that the

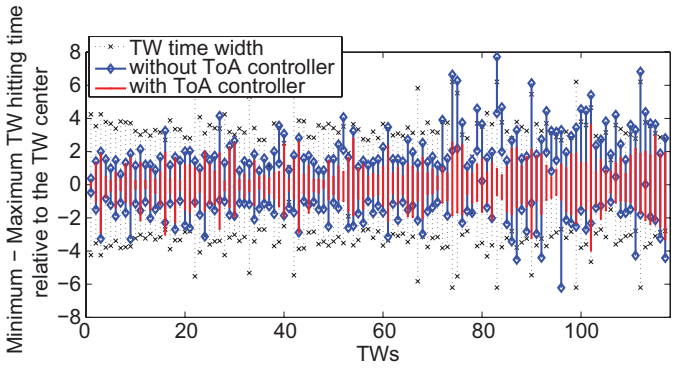

Fig. 9. Minimum and maximum TW hitting times for each TW, relative to the TW center. For visualization purposes, all TW are shifted so that they are centered to zero. The red bars (with point extremities) correspond to the case where time of arrival control is used, whereas the blue bars (with diamond extremities) depict the uncontrolled case; the extremities correspond to the minimum and maximum TW hitting times. As a result of the improvement afforded by the use of time of arrival control, the spread of the red is less than the one of the uncontrolled case. The black crosses denote the extremities of the TW's time width, as this was designed for the CATS HIL experiments.

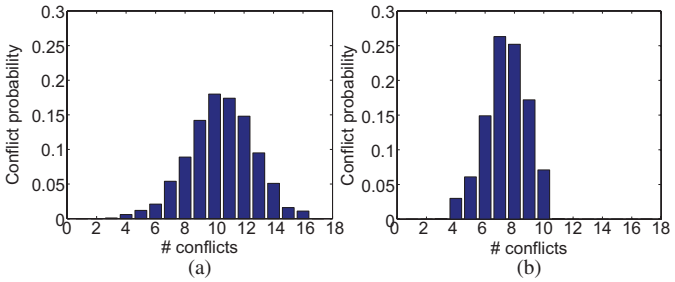

Fig. 10. Conflict probability distribution after 1000 Monte Carlo simulations for the case where uncertainty in the wind, the mass, and the time an aircraft enters the control sector are considered. (a) Without time of arrival control. (b) With time of arrival control.

extremities of each bar might correspond to outliers, and the probability distribution might be skewed differently. The actual TW hitting probability distributions for some of the simulated TW can be found in [9].

C. Reachability Calculations

For the 50 simulated flights, we performed conflict detection so as to identify the flights with high conflict probability. We considered the case where wind, mass, and entry time uncertainty are present, and carried out 1000 Monte Carlo simulations with and without time of arrival control. Fig. 10(a) depicts the conflict probability distribution for the case where no time of arrival control is used. We encountered a median of ten conflicts, whereas if a time of arrival controller is employed, the median number of conflicts is reduced to seven [see Fig. 10(b)]. In general, using a time of arrival controller improves the punctuality of the flights with respect to their schedule and reduces the along track error, but does not necessarily lead to a lower number of conflicts.

Based on the conflict statistics of Fig. 10(b) (with time of arrival control), we selected the pairs of flights that are most likely to be involved in a conflict, and carried out the reachability computation outlined in Section III for them. Fig. 11 illustrates the two flights most likely to be in conflict

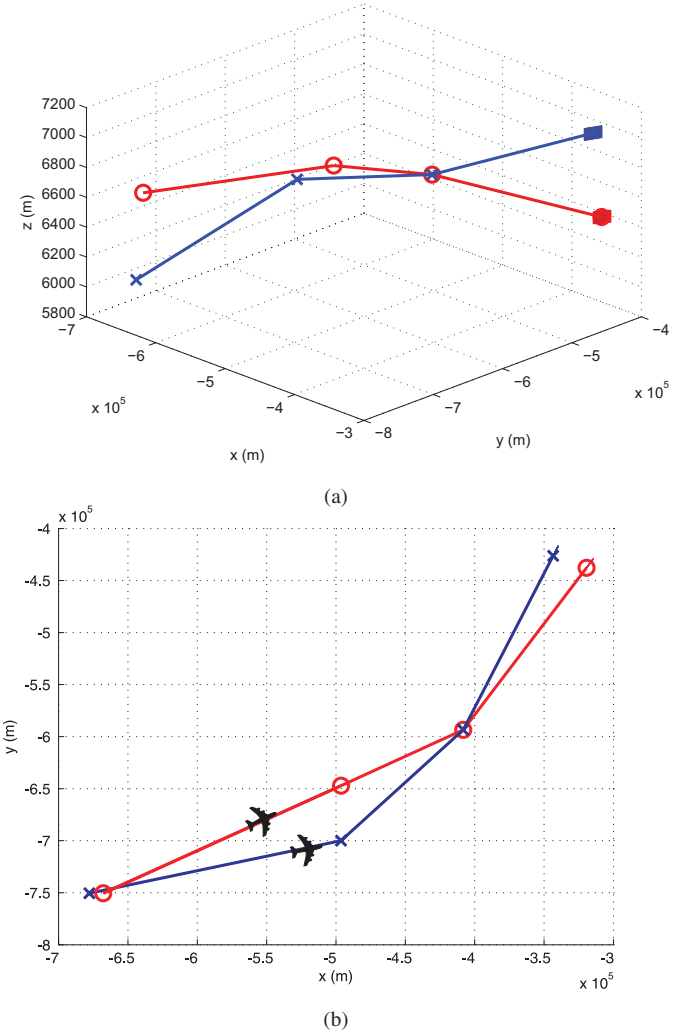

Fig. 11. (a) Flight plans for a two aircraft scenario. The red and blue rectangles represent the TWs of each flight. (b) Flight plan top view for the same two aircraft case. Note that for the reachability calculations, the projection of the TWs on the horizontal plane is line segments, which are aligned with the flight plan.

close to their third way point. The TWs are centered at the last way point of each flight plan. For comparison purposes, Fig. 12(a) and (b) shows a snapshot of the two-stage backward reachability computation, i.e., if the avoid region is the empty set. The tubes at this figure include all the states that each aircraft could start from and fulfill its TW constraints, ignoring for the time being the fact that there may be conflicts along the way. Since aircraft fly faster at higher flight levels, there are more states that can reach each TW at high altitudes. The numerical values next to the way points in Fig. 12(b) indicate the corresponding altitude. Note that the x-y projection of the reachable tubes coincides with the projection of the flight plans on the horizontal plane [Fig. 11(b)], since in the hybrid model we assumed perfect lateral tracking.

Fig. 12(c) shows the same set, after removing all points where the two aircrafts are in conflict at some time instance. For each aircraft j, the hole around the intersection point is the union of all "avoid" regions $A_{j,t}$. For a better understanding, Fig. 13 shows the reach-avoid tubes on the $s-z$ plane, as well as the time evolution of the conflict zone of each aircraft

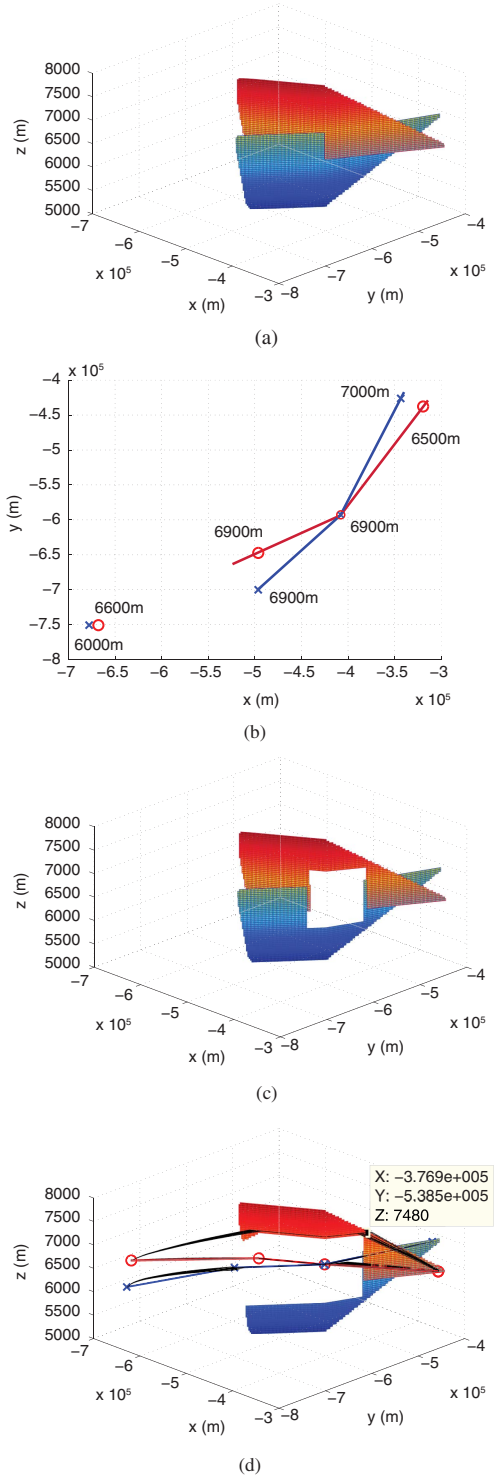

Fig. 12. (a) Backward reachable tubes, including all states from which each aircraft can reach its TW. (b) Projection of the reachable tubes on the horizontal plane. The values next to the way points indicate the corresponding altitude. (c) Conflict zone including all states that are in conflict at some time instance, calculated based on the minimum separation standards. (d) Reach-avoid tubes calculated via Algorithm 1. The black lines correspond to sample simulated trajectories, after introducing an artificial TW.

for four time instances separated by 3 minutes. These sets can be thought of as level sets of the time-dependent obstacle function $h_j(x_j, t)$ at four different time instances.

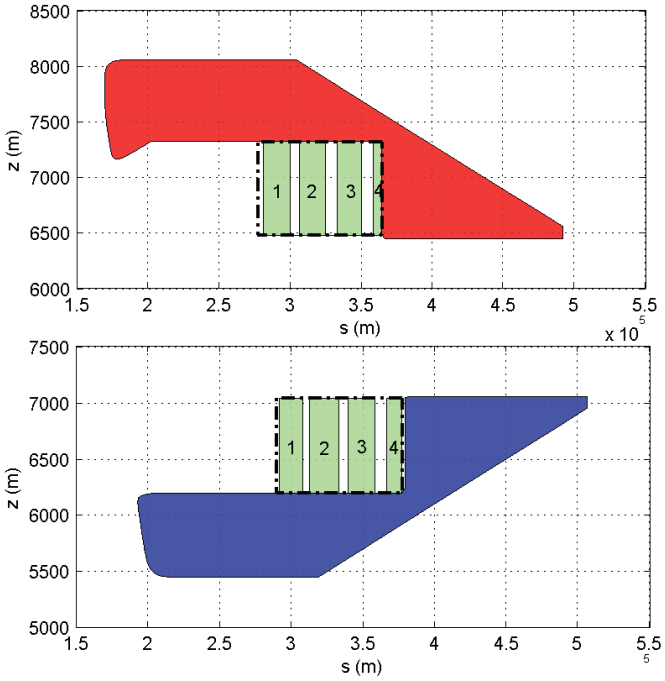

Fig. 13. Reach-avoid tubes and time evolution of the conflict zone for the aircraft of Fig. 12 in the $s - z$ plane, for four time instances separated by 3 minutes. The green regions denote the conflict zones, whereas the numbering indicates the sets of states for each aircraft that are in conflict at the same time instance. The dotted rectangles denote the boundary of the conflict zone for each aircraft of Fig. 12(c) on the $s - z$ plane.

By applying now the reach-avoid approach of Section III-C, we can construct the conflict free tubes of Fig. 12(c). As expected, the set of states that could reach the target while avoiding conflict with the other aircraft, excludes the conflict zone of Fig. 12(c), as well as all other states that would end up in this zone for some wind realizations irrespective of the control inputs of the hybrid automaton.

The reach-avoid tubes provide an indication of the locations where aircraft can be and avoid conflict while meeting their TW constraints. An air traffic controller can then use this information to reroute the flight. To illustrate how this can be done, we place an artificial TW inside the reach-avoid tubes of Fig. 12(d) by hand.

An air traffic controller could do something similar given the information generated by the reachability calculation. They could also issue standard maneuvers, e.g., vectoring or flight level changes, leading to changes in the flight plan. In this case, the reachability calculation can be repeated for the new flight plan providing feedback to the air traffic controller whether the proposed maneuver resolves the conflict and respects the existing TW constraints. The updated flight plan with the new TW sequence is imported in the detailed simulation environment of Section II-A and is tracked by the FMS, which is equipped with the time of arrival controller of Section II-C. We then run Monte Carlo simulations considering again uncertainty in the wind, the mass, and the time an aircraft enters the control sector, to evaluate the effect of this action had on the probability of conflict.

We applied this procedure to the three pairs of flights with the highest conflict probability, but any conflict resolution

TABLE I
PROBABILITY OF CONFLICT

	Prior to Resolution	After Resolution
Case 1	100%	0%
Case 2	100%	0%
Case 3	99%	15%

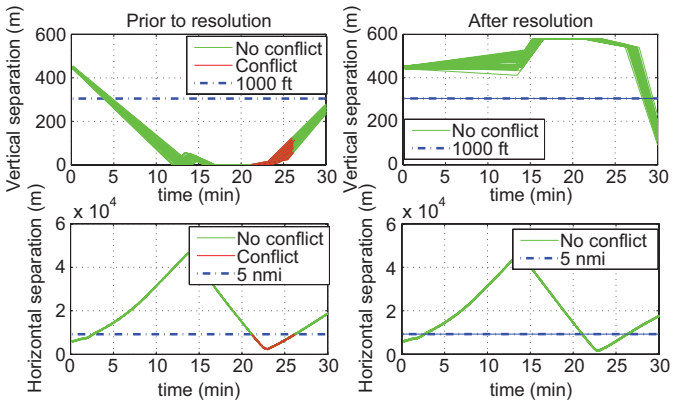

Fig. 14. Time evolution of the horizontal and vertical separation between the two aircrafts of Fig. 11 for different uncertainty realizations, before and after the proposed resolution maneuver (left and right panels, respectively). The red line segments correspond to time instances where a conflict is encountered, whereas green lines represent cases where a safe separation is achieved. The blue dotted lines indicate the minimum distance values that ensure safe separation.

algorithm from the literature could have been used instead to identify dangerous encounters. The results are summarized in Table I. Case 1 corresponds to the two aircrafts example of Fig. 12, where one of the aircraft was rerouted by placing a 2 minute TW at the position shown in Fig. 12(d). The black lines in Fig. 12(d) represent 20 sample simulated trajectories (out of 1000 Monte Carlo simulations), which correspond to different uncertainty realizations. For the case where no resolution was performed, the simulated tracks follow closely the nominal flight plans, deviating slightly at the "climb" and "descent" phase as expected. In the case where a maneuver is initiated, all simulated trajectories pass from the artificial TW and no conflict occurs. Fig. 14 shows the time evolution of the horizontal and vertical separation between the two aircrafts for different uncertainty realizations, before and after the proposed resolution maneuver (left and right panels, respectively). After the resolution maneuver of Fig. 12(d), no conflict is encountered.

Despite the fact that the reachability analysis assumed a worst case setting, with the wind acting as a bounded disturbance input, the probability of conflict in case 3 of Table I is not reduced to zero. This is justified by the fact that the rerouted track was computed based on the reach-avoid tubes, which include only bounded wind uncertainty, whereas the maneuver was executed on the detailed simulator of Section II, and in the presence of wind, mass, and entry time uncertainty.

D. Computational Issues

All simulations were performed on an Intel(R) Core(TM)2 Duo 2.66 GHz processor running Windows 7. The reachability calculations were implemented using the level set method Toolbox [53] (version 1.1) on MATLAB 7.10. Since the terminal sets (the TWs) are small compared to the simulated space, a 501×501 grid was used initially to avoid degeneracy. When the sets had increased enough, the grid was changed to 251×251 to increase the computational efficiency. Specifically, for the two aircrafts example (25 minutes of flight) of Fig. 12, 8.22 minutes were needed to complete the reachability computation, whereas the memory usage of MATLAB was 744 MB. The Monte Carlo simulations of the 50 flights of Fig. 6 were carried out in the detailed simulation environment of Section II-A, which is coded in JAVA, with a MATLAB interface. Every simulation (for all flights) required $\sim$9.3 s, and $\sim$2 MB memory.

V. CONCLUSION

In this paper, a novel concept for 4-D trajectory management in air traffic control, based on the notion of TWs, was evaluated via Monte Carlo simulations in terms of the TW hitting and conflict probability. An abstraction of the aircraft dynamics was performed, and a reachability based algorithm to compute the maneuvering bounds of each aircraft in the presence of TW constraints was developed and tested via Monte Carlo simulations. A resolution procedure was then carried out, based on placing artificial TWs on the reach-avoid tubes. Indeed, the TW placement was effectively done by hand, showing how an air traffic controller could make use of the information provided by the reachability calculation.

In the current implementation, no optimization was employed when placing the artificial TWs in the reach-avoid tubes. Moreover, we treated each conflict pair separately without considering the possibility that the resolution command causes subsequent conflicts. For a more realistic implementation, vectoring commands should also be taken into account. We do not propose a conflict resolution algorithm per se, this is the topic of future work.

ACKNOWLEDGMENT

The authors would like to thank A. Lotz and S. Guibert for their valuable input and insight in the current work, and the anonymous reviewers for their constructive comments that significantly improved the presentation of this paper.

REFERENCES

[1] *SESAR Definition Phase - Deliverable D1 - Air Transport Framework - The Current Situation*. (2006, Jul.) [Online]. Available: http://www.eurocontrol.int/sesar/public/standard_page/documentation.html

[2] *Next Generation Air Transportation System (NGATS) Air Traffic Management (ATM) - Airportal Project*. (2007, May) [Online]. Available: http://www.aeronautics.nasa.gov/nra_pdf/airspace_project_c1.pdf

[3] *SESAR The ATM Target Concept - Deliverable D3*. (2006, Dec.) [Online]. Available: http://www.eurocontrol.int/sesar/public/standard_page/documentation.html

[4] *CATS State of the Art - Deliverable D1.1*. (2008, Jun.) [Online]. Available: http://www.cats-fp6.aero/cats-fp6/public_deliverables.html

[5] *Validation Strategy and Plan - Deliverable D1.3.1*. (2008, Dec.) [Online]. Available: http://www.cats-fp6.aero/cats-fp6/public_deliverables.html

[6] *Report on Target Window Modeling - Deliverable D2.2.4.3*. (2010, Oct.) [Online]. Available: http://www.cats-fp6.aero/cats-fp6/public_deliverables.html

[7] L. Castelli, L. Corolli, and G. Lulli, "Critical flights detected with time windows," *Transp. Res. Rec., J. Transp. Res. Board*, vol. 2214, no. 1, pp. 103–110, 2011.

[8] *HIL2 Primary Results Analysis - Deliverable D2.1.2*. (2010, May) [Online]. Available: http://www.cats-fp6.aero/cats-fp6/public_deliverables.html

[9] *Report on Modelling and Quantitative Risk Analysis - Deliverable D2.2.1.2*. (2010, Jul.) [Online]. Available: http://www.cats-fp6.aero/cats-fp6/public_deliverables.html

[10] A. Lecchini-Visintini, J. Lygeros, and J. Maciejowski, "Monte Carlo optimization for conflict resolution in air traffic control," *IEEE Trans. Intell. Transp. Syst.*, vol. 7, no. 4, pp. 470–482, Dec. 2006.

[11] H. Blom, J. Krystul, and G. Bakker, "A particle system for safety verification of free flight in air traffic," in *Proc. IEEE Conf. Decision Control*, Mar. 2007, pp. 1574–1579.

[12] H. Blom, G. Bakker, B. K. Obbink, and M. Klompstra, "Free flight safety risk modeling and simulation," in *Proc. 2nd Int. Conf. Res. Air Transp.*, 2006, pp. 1–10.

[13] G. Chaloulos and J. Lygeros, "Effect of wind correlation on aircraft conflict probability," *AIAA J. Guidance, Control, Dynamics*, vol. 30, no. 6, pp. 1742–1752, 2007.

[14] R. Paielli and H. Erzberger, "Conflict probability estimation for free flight," *AIAA J. Guidance, Control, Dynamics*, vol. 20, no. 3, pp. 588–596, 1997.

[15] R. Paielli and H. Erzberger, "Conflict probability estimation generalized to non-level flight," *Air Traffic Control Quart.*, vol. 7, no. 3, pp. 195–222, 1999.

[16] C. Tomlin, J. Lygeros, and S. Sastry, "A game theoretic approach to controller design for hybrid systems," *Proc. IEEE*, vol. 88, no. 7, pp. 949–969, Jul. 2000.

[17] K. Margellos and J. Lygeros, "Hamilton–Jacobi formulation for reach–avoid differential games," *IEEE Trans. Autom. Control*, vol. 56, no. 8, pp. 1849–1861, Aug. 2011.

[18] C. Tomlin, G. Pappas, and S. Sastry, "Conflict resolution for air traffic management: A study in multiagent hybrid systems," *IEEE Trans. Autom. Control*, vol. 43, no. 4, pp. 509–521, Apr. 1998.

[19] M. Oishi, I. Mitchell, A. Bayen, and C. Tomlin, "Invariance-preserving abstractions of hybrid systems: Application to user interface design," *IEEE Trans. Control Syst. Technol.*, vol. 16, no. 2, pp. 229–244, Mar. 2008.

[20] C. Tomlin, J. Lygeros, and S. Sastry, "Aerodynamic envelope protection using hybrid control," in *Proc. Amer. Control Conf.*, 1998, pp. 1793–1796.

[21] J. Lygeros, C. Tomlin, and S. Sastry, "Controllers for reachability specifications for hybrid systems," *Automatica*, vol. 35, no. 3, pp. 349–370, 1999.

[22] A. M. Bayen, I. M. Mitchell, M. Oishi, and C. Tomlin, "Aircraft autolander safety analysis through optimal control-based reach set computation," *J. Guidance, Control, Dynamics*, vol. 30, no. 1, pp. 68–77, 2007.

[23] I. Kitsios and J. Lygeros, "Final glide-back envelope computation for reusable launce vehicle using reachability," in *Proc. IEEE Conf. Decision Control*, Dec. 2005, pp. 4059–4064.

[24] E. Cruck and J. Lygeros, "Subliminal air traffic control: Human friendly control of a multiagent system," in *Proc. Amer. Control Conf.*, 2007, pp. 462–467.

[25] J. Aubin, *Viability Theory*. Boston, MA: Birkhäuser, 1991.

[26] P. Cardaliaguet, "A differential game with two players and one target," *SIAM J. Control Optim.*, vol. 34, no. 4, pp. 1441–1460, 1996.

[27] P. Cardaliaguet, M. Quincampoix, and P. Saint-Pierre, "Pursuit differential games with state constraints," *SIAM J. Control Optim.*, vol. 39, no. 5, pp. 1615–1632, 2001.

[28] M. Bardi and I. Capuzzo-Dolcetta, *Optimal Control and Viscosity Solutions of Hamilton–Jacobi–Bellman Equations*. Boston, MA: Birkhäuser, 1997.

[29] P. Cardaliaguet, M. Quincampoix, and P. Saint-Pierre, "Set valued numerical analysis for optimal control and differential games," in *Annals of the International Society of Dynamic Games*, vol. 4, M. Bardi, T. Raghaven, and T. Papasarathy, Eds. Boston, MA: Birkhäuser, 1999, pp. 177–247.

[30] J. P. Aubin, J. Lygeros, M. Quincampoix, S. Sastry, and N. Seube, "Impulse differential inclusions: A viability approach to hybrid systems," *IEEE Trans. Autom. Control*, vol. 47, no. 1, pp. 2–20, Jan. 2002.

[31] Y. G. Gao, J. Lygeros, and M. Quincampoix, "On the reachability problem for uncertain hybrid systems," *IEEE Trans. Autom. Control*, vol. 52, no. 9, pp. 1572–1586, Sep. 2007.

[32] I. J. Fialho and T. Georgiou, "Worst case analysis of nonlinear systems," *IEEE Trans. Autom. Control*, vol. 44, no. 6, pp. 1180–1196, Jun. 1999.

[33] J. Lygeros, "On reachability and minimum cost optimal control," *Automatica*, vol. 40, no. 6, pp. 917–927, 2004.

[34] I. Mitchell, A. M. Bayen, and C. Tomlin, "Validating a Hamilton Jacobi approximation to hybrid reachable sets," in *Hybrid Systems: Computation and Control*, M. Di Benedetto and A. Sangiovanni-Vincentelli, Eds. New York: Springer-Verlag, 2001, pp. 418–432.

[35] I. Mitchell, A. M. Bayen, and C. Tomlin, "A time-dependent Hamilton–Jacobi formulation of reachable sets for continuous dynamic games," *IEEE Trans. Autom. Control*, vol. 50, no. 7, pp. 947–957, Jul. 2005.

[36] L. C. Evans and P. E. Souganidis, "Differential games and representation formulas for solutions of Hamilton–Jacobi–Isaacs equations," *Indiana Univ. Math. J.*, vol. 33, no. 5, pp. 773–797, 1984.

[37] S. Osher and J. Sethian, "Fronts propagating with curvature-dependent speed: Algorithms based on Hamilton–Jacobi formulations," *J. Comput. Phys.*, vol. 79, no. 1, pp. 12–49, 1988.

[38] J. A. Sethian, *Level Set Methods: Evolving Interfaces in Geometry, Fluid Mechanics, Computer Vision, and Materials Science*. New York: Cambridge Univ. Press, 1996.

[39] I. M. Mitchell, "Application of level set methods to control and reachability problems in continuous and hybrid systems," Ph.D. dissertation, Dept. Comput. Sci., Stanford Univ., Stanford, CA, Feb. 2002.

[40] I. Mitchell and C. Tomlin, "Level set methods for computation in hybrid systems," in *Hybrid Systems: Computation and Control*, N. Lynch and B. Krogh, Eds. New York: Springer-Verlag, 2000, pp. 310–323.

[41] K. Margellos and J. Lygeros, "Air traffic management with target windows: An approach using reachability," in *Proc. IEEE Conf. Decision Control*, Mar. 2009, pp. 145–150.

[42] K. Margellos and J. Lygeros, "Hamilton–Jacobi formulation for reach-avoid problems with an application to air traffic management," in *Proc. Amer. Control Conf.*, 2010, pp. 3045–3050.

[43] *User Manual for the Base of Aircraft Data (BADA) Revision 3.3*. (2002) [Online]. Available: http://www.eurocontrol.fr/projects/bada/

[44] I. Lymperopoulos, J. Lygeros, A. Lecchini, W. Glover, and J. Maciejowski, "A stochastic hybrid model for air traffic management processes," Dept. Eng., Univ. Cambridge, Cambridge, U.K., Tech. Rep. AUT07-15, 2007.

[45] W. Glover and J. Lygeros, "A stochastic hybrid model for air traffic control simulation," in *Hybrid Systems: Computation and Control*, R. Alur and G. Pappas, Eds. New York: Springer-Verlag, 2004, pp. 372–386.

[46] I. Lymperopoulos, "Sequential Monte Carlo methods in air traffic management," Ph.D. dissertation, ETH, Zürich, Switzerland, 2010.

[47] I. Lymperopoulos and J. Lygeros, "Improved multi-aircraft ground trajectory prediction for air traffic control," *AIAA J. Guidance, Control, Dynamics*, vol. 33, no. 2, pp. 347–362, 2010.

[48] I. Lymperopoulos and J. Lygeros, "Sequential Monte Carlo methods for multi-aircraft trajectory prediction in air traffic management," *Int. J. Adapt. Control Signal Process.*, vol. 24, no. 10, pp. 830–849, 2010.

[49] M. R. C. Jackson, "Sensitivity of trajectory prediction in air traffic management and flight management systems," Ph.D. thesis, Dept. Electr. Eng., Univ. Minnesota, Minneapolis, 1997.

[50] M. Jackson, V. Sharma, C. Haissig, and M. Elgersma, "Airborne technology for distributed air traffic management," in *Proc. IEEE Conf. Decision Control*, Feb. 2005, pp. 3947–3954.

[51] A. Lotz, "Implementation and performance evaluation of time of arrival control for air traffic management," Ph.D. thesis, ETH, Zürich, Switzerland, 2009.

[52] P. P. Varaiya, "On the existence of solutions to a differential game," *SIAM J. Control Optim.*, vol. 5, no. 1, pp. 153–162, 1967.

[53] I. Mitchell, "A toolbox of level set methods," Dept. Comput. Sci., UBC, Vancouver, BC, Canada, Tech. Rep. TR-2007-11, 2007.

[54] A. Vladimirsky, "Static PDEs for time-dependent control problems," *Interf. Free Bound.*, vol. 8, no. 3, pp. 281–300, 2006.

[55] *Advanced Required Navigation Performance (A-RNP) Real-Time Simulation*. (2010, Apr.) [Online]. Available: http://www.eurocontrol.int/crds/gallery/content/public/reports/10067-CR%DSSIMRTS-FEU_01.01.pdf

[56] I. Mitchell, "Comparing forward and backward reachability as tools for safety analysis," in *Hybrid Systems: Computation and Control*, vol. 4416, A. Bemporad, A. Bicchi, and G. Buttazzo, Eds. New York: Springer-Verlag, 2007, pp. 428–443.

[57] R. E. Cole, C. Richard, S. Kim, and D. Bailey, "An assessment of the 60 km rapid update cycle (RUC) with near real-time aircraft reports," MIT Lincoln Laboratory, Lexington, Tech. Rep. NASA/A-1, 1998.

Kostas Margellos (S'09) received the Diploma degree in electrical and computer engineering from the University of Patras, Patras, Greece, in 2008. He is currently pursuing the Ph.D. degree in automatic control with ETH Zürich, Zürich, Switzerland.

His current research interests include reachability analysis and control of nonlinear and hybrid systems, with applications to complex networks such as power grids with uncertain generation and collision avoidance algorithms in air traffic management.

John Lygeros (S'91–M'97–SM'06–F'11) received the B.Eng. degree in electrical engineering and the M.Sc. degree in systems control from the Imperial College of Science Technology and Medicine, London, U.K., in 1990 and 1991, respectively, and the Ph.D. degree in electrical engineering and computer sciences from the University of California (UC), Berkeley, in 1996.

He held a series of research positions with the National Automated Highway Systems Consortium, the Massachusetts Institute of Technology, Cambridge, and UC Berkeley from 1996 to 2000. He was a part-time Research Engineer with SRI International, Menlo Park, CA, and was a Visiting Professor with the Department Mathematics, Universite de Bretagne Occidentale, Brest, France. From 2000 to 2003, he was a Lecturer with the Department of Engineering, University of Cambridge, Cambridge, U.K. From 2003 to 2006, he was an Assistant Professor with the Department of Electrical and Computer Engineering, University of Patras, Patras, Greece. In 2006, he joined the Automatic Control Laboratory, ETH Zürich, Zürich, Switzerland, where he is currently the Head. His current research interests include modeling, analysis, and control of hierarchical, hybrid, and stochastic systems, with applications to biochemical networks, air traffic management, power grids, and camera networks.

Dr. Lygeros was a fellow of Churchill College.